



UNIVERSITÀ DI PARMA

ARCHIVIO DELLA RICERCA

University of Parma Research Repository

A 10-mA LDO With 16-nA IQ and Operating From 800-mV Supply

This is the peer reviewed version of the following article:

Original

A 10-mA LDO With 16-nA IQ and Operating From 800-mV Supply / Adorni, N.; Stanzione, S.; Boni, A.. - In: IEEE JOURNAL OF SOLID-STATE CIRCUITS. - ISSN 0018-9200. - 55:2(2020), pp. 404-413. [10.1109/JSSC.2019.2948820]

Availability:

This version is available at: 11381/2865950 since: 2021-12-15T11:59:51Z

Publisher:

Institute of Electrical and Electronics Engineers Inc.

Published

DOI:10.1109/JSSC.2019.2948820

Terms of use:

Anyone can freely access the full text of works made available as "Open Access". Works made available

Publisher copyright

note finali coverpage

(Article begins on next page)

13 August 2025

A 10mA LDO with 16nA-IQ and operating from 800 mV supply

Nicola Adorni, Stefano Stanzione, and Andrea Boni

Abstract—A low dropout regulator (LDO) with a quiescent current in the tens of nA range and operating from 800 mV supply is proposed. A rail-to-rail buffer with zero I/O voltage shift and based on the differential flipped voltage follower is used for combined gate and bulk driving of the output device. Therefore, bulk modulation with forward-body bias is implemented without any additional amplifier. The proposed buffer is a crucial block for the sub-1 V supply and for limiting the contribution of the output device to the quiescent current. The error amplifier is adaptively biased with a bias shaper block, which implements a current limiting at high loads and a linear dependence on the output current at moderate loads. The feedback signal for the bias control is the output of the amplifier instead of the gate voltage of the pass device, thus combining a nA bias at light load with the ability to follow a fast output current transient. Finally, a corner-tracking load is used to set the bias current of the output device to the minimum value at the target stability margin, over the temperature and process parameters space.

The LDO was implemented in a 55 nm CMOS technology. The measured quiescent current is 16 nA, with a minimum Power Supply Rejection of 42.7 dB up to 50 kHz and a maximum load current of 10 mA. In order to compare the transient behavior of state-of-the-art designs, a modified figure-of-merit is proposed, taking into account the penalty caused by the low supply.

Index Terms— Low dropout regulators, CMOS LDO, Adaptive bias, Bulk modulation, Forward body-bias, Rail-to-Rail buffer, Low-quiescent current, Low-voltage, Tracking compensation.

I. INTRODUCTION

Battery-powered devices for Internet of Things (IoT) applications, remote sensing, and implantable or wearable biomedical equipment require extremely efficient power management circuits for extending the battery life or eventually enabling autonomous operation with energy harvesting [1], [2].

For power saving reasons, those devices generally operate in duty cycle mode, hence periodically switching from standby to the on-state. Additionally, in recent years, a number of electronic systems consuming a few μA have been realized, pushing the power management blocks to consume a negligible fraction of the total system consumption. A logical consequence is that power management circuits must be able to operate at a very low output current, maintaining a safe stability margin of the involved feedback loops and high

current efficiency. Therefore, a low quiescent current (I_Q) in the hundreds nA is required.

An additional requirement is to have a fast transient performance, capable to cope with the turn-on of load circuits recovering from the sleep mode. Furthermore, the low-voltage operation is becoming a mandatory feature of power management circuits. A trend of reduction of the load circuits voltage supply is forced by the need for consuming less power [3]. It is important to note that this trend is valid also for analog circuits. However, sensitive analog circuits require low-dropout regulators (LDO), which provide a stable supply voltage from a higher, unregulated or dirty, input [4]. LDOs are efficient only if the input voltage is close to the output voltage. This means that also such LDO will need to be correctly operating at very low supply voltages (under 1 V).

An additional feature that is often overlooked is the kickback noise related to a wide and fast transient of the load current. Indeed, in ultra-low-power designs the voltage reference circuit, providing the set-point for the regulation of the supply voltage, is usually unbuffered, thus extremely

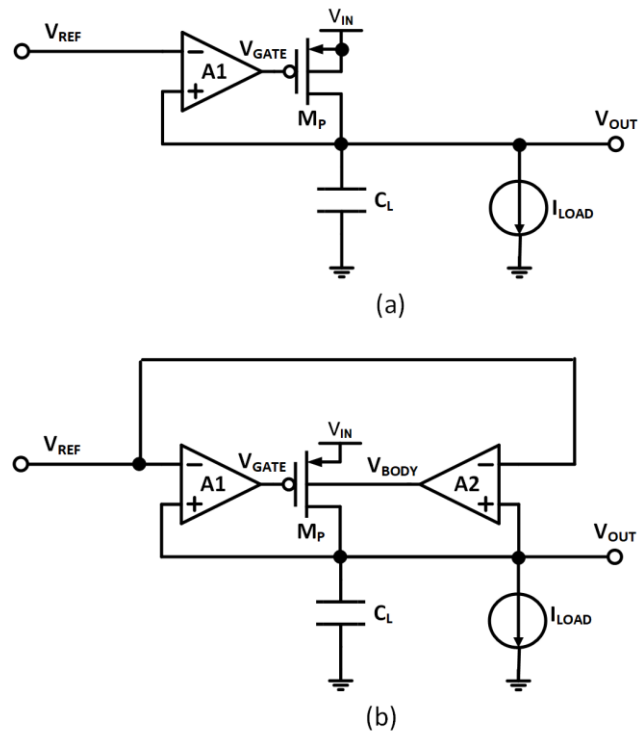


Fig. 1. Black-box schematic of LDO with unity gain feedback: (a) without body bias control and (b) with bulk-modulation.

N. Adorni was with Holst Centre / imec-NL, 5656 AE Eindhoven, The Netherlands, and also with University of Parma, I-43124, Parma, Italy

S. Stanzione is with the Connected Health Solutions department of Holst Centre / imec, High Tech Campus 31, 5656 AE, Eindhoven, The Netherlands (e-mail: stefano.stanzione@imec.nl).

A. Boni is with the Department of Engineering and Architecture, University of Parma, Parco Area delle Scienze, 181/A, I-43124, Parma, Italy (e-mail: andrea.boni@unipr.it).

exposed to cross-talk, coupled to its output. A possible attenuation of this problem consists in integrating a large decoupling capacitor, but this implies an excessive Silicon area.

A black-box schematic of a generic LDO with unity gain feedback is reported in Fig. 1(a). A critical design aspect is the stability margin, which is severely affected by the load capacitance of the error amplifier A1, due to the gate of the pass device, M_P . Adequate compensation is either achieved by means of a large off-chip or an internal capacitor or both, while a buffer with a low output impedance is often introduced [5], [6] between the amplifier and the pass device.

Other relevant specifications of this circuit are the load and the line regulation. The former is a relevant parameter if the load current undergoes large variations because of the activity of the logic circuits and the periodic change of state of the wireless device. The latter is a crucial parameter for maintaining the regulated supply during almost all the battery discharge or with an energy harvesting source.

The above requirements raise several design problems that were addressed with various approaches in state-of-the-art designs reported in the literature. In [7] the bulk voltage of the output transistor is controlled by a separate feedback loop to improve the load and line regulation together with the stability margin. The modification of the basic architecture is shown in Fig. 1(b), where an additional amplifier, featuring a moderate voltage gain and a large bandwidth, is used for driving the bulk of the pass device. Nevertheless, this amplifier increases the quiescent current of the regulator. In [8] the forward body bias (FBB) was implemented for the output device to reduce the gate area and improve the regulation characteristics. An additional circuit, not reported in that paper, is required, thus leading to additional power consumption. Furthermore, the extensive usage of cascoding in the error amplifier severely affects the minimum input voltage that is indeed limited to 2.8 V.

In order to strongly reduce the quiescent current, in particular with a light load, adaptive bias was proposed for the error amplifier and the buffer [5], [6], [9]. In [5] a minimum quiescent current as low as 0.9 μA was achieved by making the bias current of the single-stage amplifier dependent on the gate voltage of the pass device. This solution may suffer from a slow transient in the case of a positive step of the load current, because of the large gate capacitance of that device. This problem was avoided with an enhanced current mirror buffer. The limits of this implementation are twofold: the quiescent current is not upper limited by design and the output buffer does not exhibit a rail-to-rail output. The former characteristic is prone to cause an excessive kickback noise at the reference input. The latter limits the maximum source-gate voltage of the pass device. In [6] an impressive transient time was achieved by means of a high-speed super current mirror, which drives the pass device and controls the adaptive bias. However, the added complexity of the buffer design, based on three branches, leads to a minimum I_Q well above 1 μA .

In [10] a cap-less LDO (i.e. without off-chip compensation capacitance) featuring 100 nA I_Q at 1 V input and with a minimum 100 nA load is presented. Besides the typical adaptive bias circuit driven by the gate voltage of the pass device, a dynamic bias current generator is added. The drop-

out voltage is monitored and used to enable the additional bias current. Therefore, the I_Q is expected to strongly depend on the unregulated input voltage.

This regulator is based on the flipped-voltage-follower (FVF) topology with a folded-cascode gain stage [11]. In such LDOs the pass device is embedded in the FVF and it corresponds to the upper PMOS in the common-source configuration [12]. The gain provided by the folded-cascode stage allows removing the error amplifier, with some power saving, at the cost of a worse Power Supply Rejection (PSR). Moreover, it is worth to notice that cap-less LDOs usually exhibit larger under/overshoot in the presence of a fast transition time of the load current.

Furthermore, in [13] an LDO design featuring 1 μA minimum I_Q is reported. The regulator is based on an NMOS output device, which hence requires an internal charge pump for achieving a similar drop-out than PMOS-based regulators. The complexity of the circuit generating the adaptive bias and the multi-branch buffer severely limit the scaling of the quiescent current, that can be hardly reduced to hundreds of nA. Furthermore, the minimum input voltage is limited to 1.5 V, and high-voltage devices (7 V) are required.

A different approach is proposed in [14] where the power efficiency of the LDO is maximized at high load by keeping the minimum drop-out as low as 50 mV. This was achieved with a self-supplied error amplifier that limits the PSR degradation. However, the relatively large I_Q makes this design not suitable for duty-cycled systems, where the regulator works for most of the time in light-load conditions.

Extending the survey to low- I_Q LDOs available on the market, a quiescent current as low as 500 nA is achieved by [15], but the minimum input voltage is 2.2 V and the PSR in the 0-50 kHz range is very low, i.e. lower than 10 dB at 1mA load.

Therefore, on the basis of the survey of state-of-the-art designs reported in the literature, and on the authors' knowledge, no LDO design achieving all the required specs for pushing the performance of low-power devices, was reported.

The design target of the LDO discussed in the paper was to simultaneously achieve a quiescent current of few tens of nA, a sub-1 V minimum input voltage, a strong line regulation, and a minimum PSR of about 40 dB up to few tens of kHz. The targets were achieved by extending the concept of the adaptive bias to all the involved blocks, thus leading to a super-adaptive LDO, and by an innovative implementation of the concurrent bulk-modulation and FBB of the pass device. Unlike the reported implementations, the bias current of the error amplifier is almost linearly dependent on the load current and it is upper limited by design, leading to an almost

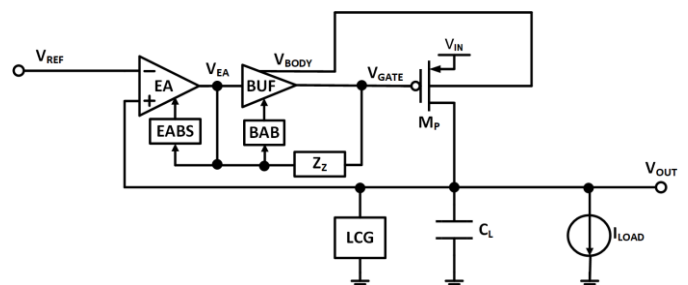


Fig. 2. Black box schematic of the proposed LDO.

requirement for a sub-1 V operation calls for alternative design strategies to cascoding. Therefore, the output stage of the amplifier (M₈-M₁₀) is implemented as a rail-to-rail complementary common-source, whereas the local positive feedback with a cross-coupled PMOS load (M₃-M₄) boosts the DC gain of the first stage, without affecting the output range [16], [17]. Notice that bias currents I_{B1}, I_{B2} and also I_{BL} and I_{BH} (in Fig. 5) are all generated by mirroring an input current reference provided externally.

The transfer function of the error amplifier exhibits two non-dominant poles:

$$p_{A1} = -\frac{g_{m5} - g_{m3}}{C_{gs5} + C_{gs3}} \quad (1)$$

$$p_{A2} = -\frac{g_{m9}}{C_{gs9} + C_{gs10}} \quad (2)$$

where C_{gs<i>} and g_{m<i>} are the gate-source capacitance and small-signal transconductance of M_{<i>}, and any random mismatch has been neglected. The pole p_{A1} is pushed to a higher frequency, without affecting the voltage gain of EA, by reducing the width of M₃-M₆, at a fixed current, provided that the involved devices are maintained in Weak-Inversion (W.I.). However, this lowers the DC voltage at the drain of M₁-M₂, thus reducing the common-mode input range of the error amplifier. To relax the latter constraint, the FBB is exploited by sharing the same body bias with the pass device. It is worth to notice that the stability constraints of the LDO dictate that such non-dominant poles are always well above the unity-gain frequency (UGF) of the LDO loop gain, as discussed in Section IV.

A. Buffer with Adaptive Bias and Embedded Body Bias Generation

If the buffer exhibits a significant I/O voltage shift, the rail-to-rail output range of the error amplifier is underused. For the same reason, also the buffer must feature an almost rail-to-rail behavior and properly operate with a sub-1 V supply voltage. To this aim, a Differential Flipped-Voltage-Follower (DFVF) has been used, M₁₁-M₁₆ [12]. This circuit is based on an input side (M₁₃, M₁₅, M₁₇) with negative feedback through device M₁₇ for achieving a low output resistance at the source of M₁₅ and M₁₆. By means of the output branch (M₁₄, M₁₆) an almost zero voltage shift is obtained, at the cost of increased output resistance of the buffer, R_{ob}, with respect to the simple flipped-voltage follower (FVF):

$$R_{ob} \approx \frac{1}{g_{m17}A_{15}} + \frac{1}{g_{m16}} \quad (3)$$

where A₁₅ = g_{m15} · r_{ds15} is the intrinsic voltage gain of M₁₅, with r_{ds15} the drain-source small-signal resistance. The above equation is rewritten considering that the involved devices are sized for weak inversion (W.I.) bias, up to the maximum I_{LOAD}:

$$R_{ob} \approx \frac{n_p \cdot v_{th}}{I_{D16}} \quad (4)$$

where I_{D<i>} is the drain current of M_{<i>}, v_{th} is the thermal voltage, n_p is the slope factor of PMOS devices, and A₁₅ >> 1 has been assumed. The contribution of the input branch, i.e. first term in (3), is negligible because of the feedback, hence

limiting the current consumption, whereas the bias current of the output branch, I_{D16}, must be set accordingly to the required value of R_{ob}. As discussed in Section IV, a higher R_{ob} does not affect the stability margin with a light load, whereas R_{ob} must decrease at high output currents. This feature is achieved with the proposed adaptively biased DFVF (ABDFVF), where the replica of the pass device, M₁₁, sets the bias currents of the buffer. Therefore, the bandwidth of the buffer at light load condition is expected to be extremely limited. Hence, a relevant delay in the low-to-high load transient is expected if V_{GATE} is used to control the gate of the replica device, as in conventional implementations. On the contrary, in the proposed adaptive bias, the output of the error amplifier, V_{EA}, is used to drive M₁₁, instead. This solution provides clear benefits to the LDO step response.

A relevant advantage of this buffer with respect to other reported LDOs is the generation of the body bias (V_{BODY}) of the output device without any additional amplifier and, therefore, any further contribution to the quiescent current. To the authors' knowledge, this is the first reported low-I_Q LDO with a DFVF used for both gate driving and bulk modulation/bias. By construction, the source-bulk voltage of M_P, V_{SBP}, is:

$$V_{SBP} = V_{SGP} - V_{SG16} \quad (5)$$

Where V_{SG<i>} is the source-gate voltage of M_{<i>} device. Since both M_P and M₁₆ are biased in W.I., the following expression for V_{SBP} is obtained:

$$V_{SBP} = n_p v_{th} \ln \left(\frac{I_{LOAD} I_{S16}}{I_{D16} I_{SP}} \right) \quad (6)$$

where I_{S<i>} is

$$I_{S<i>} = v_{th}^2 \cdot \mu_p \cdot C_d \left(\frac{W}{L} \right)_{M<i>} \cdot \exp \left(\frac{V_{T<i>}}{n_p v_{th}} \right) \quad (7)$$

with μ_p being the hole mobility, C_d the depletion capacitance, and V_{T<i>} the threshold voltage of PMOS M_{<i>} [18]. Since the bias currents of M₁₆ and M_P are linked through M₁₁ and the mirror M₁₂-M₁₃, (6) is rewritten as:

$$V_{SBP} = n_p v_{th} \ln \left(\frac{K_{16-11}}{K_{14-12}} \cdot \frac{V_{T16}}{V_{TP}} \right) + (V_{EA} - V_{GATE}) \quad (8)$$

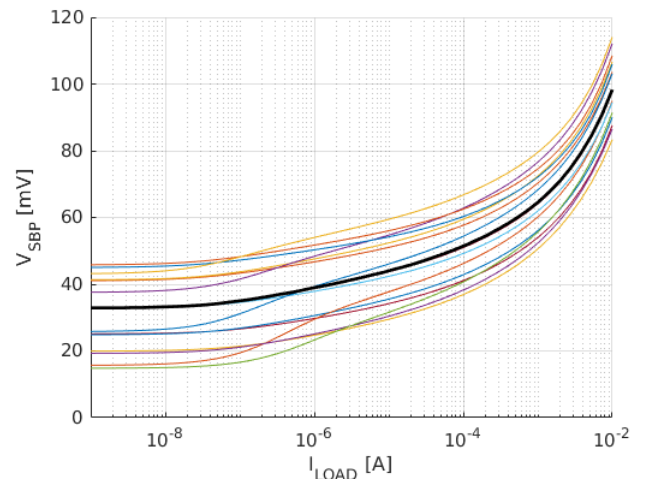


Fig. 4. Simulated source-bulk voltage of M_P over process corner, temperature, and I_{LOAD} at 0.8 V input. The thick-black line corresponds to the typical corner.

where K_{16-11} and K_{14-12} are the ratios between the W/L, of M_{16} - M_{11} , and M_{14} - M_{12} , respectively, and the effect of the different body bias of M_P and M_{16} has been taken into account. If the residual I/O shift of the buffer is neglected together with the difference of the thresholds, the body-to-source diode voltage of M_P depends only on the ratio between geometrical parameters of MOS devices. Therefore, the proposed body bias generator exhibits relevant robustness against process corner, temperature, and supply voltage.

The simulated value of V_{SBP} as a function of the load current is shown in the graph of Fig. 4. At light load, the spread of V_{SBP} over corners and temperature is within ± 15 mV with respect to the typical case. This variation is mainly due to the residual voltage shift of the buffer according to (8). Furthermore, the dependence on I_{LOAD} is negligible up to tens of μA , whereas, at higher currents, the source-bulk voltage progressively increases since M_P leaves the W.I. to enter in the moderate (M.I.) and, strong inversion (S.I.) region. Indeed, if M_P is assumed in S.I. with M_{16} in W.I., the value of V_{SBP} is roughly approximated by the overdrive voltage of the output transistor:

$$V_{SBP} \approx V_{SGP} + V_{TP} \quad (9)$$

where V_{SG16} has been assumed approximately equal to $-V_{TP}$. It is worth to notice that the value of V_{SB} is independent of the input voltage, at a fixed value of maximum I_{LOAD} . Therefore, if M_P is sized for the maximum load current at the 0.8 V input and considering a V_{TP} of about -0.5 V, we can conclude that V_{SBP} is always below the diode threshold. However, from (9) it is evident that using the ABDFVF buffer (with combined gate and bulk driving) at a sub-1 V supply severely limits the maximum FBB that can be achieved, as shown in Fig. 4. Therefore, the benefit in terms of width reduction for M_P , thanks to the body effect [18], is lower than in other designs where a dedicated circuit is used for the body bias. In the present design, the FBB provides a 20% reduction of the M_P area, with no additional quiescent current. Hence, it is evident that the area reduction thanks to FBB is here constrained by the design optimization for the lowest I_Q and by the low supply. Finally, it is worth to notice that the benefits of the bulk modulation extend to the improved load and line regulation [7].

The lower bound of the output range of the buffer is set by the saturation limit of M_{14} :

$$V_{GATEmin} = V_{DSSat14} \approx 4 \cdot v_{th} \quad (10)$$

where $V_{DSSat14}$ is the drain-source saturation voltage of M_{14} . It is worth to notice that the adaptive bias in the DFVF buffer introduces a potential risk of stability margin degradation at high-load conditions. This is due to the increased value of V_{SG17} , which reduces the drain-source voltage of M_{13} . If the saturation limit of M_{13} is exceeded downwards, (3) loses its validity, since the voltage gain of M_{15} can no longer be approximated with its intrinsic gain. Hence, the value of R_{ob} increases and the associated pole in the closed-loop transfer function is moved at a lower frequency, thus leading to a smaller phase margin or to the instability of the regulator. The issue is discussed in Section IV. Therefore, the proposed ABDFVF has to be sized for maintaining M_{13} in weak inversion and in saturation over the whole corner space.

With regard to the upper limit of the output range, it is

interesting to note that it is extended up to V_{IN} by means of the implemented adaptive bias. Indeed, with a very light load, V_{GATE} is forced to a high value to reduce the source-gate voltage of M_P , thus driving M_{17} in the triode region. Hence, the gate voltage of M_{17} decreases to maintain the same current being set by M_{13} and M_{14} . However, thanks to the adaptive bias, the current of such devices are reduced in the sub-nA range, thus limiting the variation of V_{SG17} , from the medium to the light load condition and keeping M_{13} in saturation. This condition is mandatory to maintain the current ratio I_{D14}/I_{D13} almost equal to the design value and thus to keep a unitary voltage gain and almost zero DC voltage shift. Furthermore, the adaptive bias allows achieving $V_{SG16} \ll -V_{T16}$ at light load and thus an almost rail-to-rail output capability.

$$V_{GATEmax} \approx V_{IN} \quad (11)$$

The only drawback of V_{GATE} pushed close to V_{IN} is that A_{15} in (3) is strongly reduced, leading to an increased value of R_{ob} . However, this does not impair the stability margin, because of the dependence of the dominant pole with the load current.

B. Adaptive Bias generators for the Error Amplifier

In order to achieve tens nA quiescent current, the error amplifier is adaptively biased, on the basis of the load current, as for other reported low- I_Q implementations. This solution, however, raises a few design problems. Indeed, it is hard to maintain a constant voltage gain over a wide range of bias current, leading to the degradation of DC and AC system parameters. Furthermore, a large variation of the amplifier bias current causes kickback noise at the reference input.

Such problems have been successfully addressed by means of the Error Amplifier Bias Shaper (EABS), shown in the simplified schematic of Fig. 5(a). The input of the bias block is the drain current of M_{29} , which mirrors the load current with a scaling factor equal to N . Unlike to conventional adaptive bias circuits [5], the gate of the replica device, M_{29} , is driven by the error amplifier itself, instead of the buffer, thus greatly improving the transient behavior of the bias circuit in the case of a low-to-high load current step. In addition, the load-dependent bias current is here limited by design, thus maintaining a high PSR at high load condition.

As shown in Fig. 5b, the bias current, I_{BEA} , settles to the upper bound I_{BH} at I_{LOAD} higher than I_{LTH} . This occurs when the drain current of M_{26} is higher than the saturation current of M_{30} , i.e. I_{D30sat} , and thus the mirror M_{24} - M_{25} is turned on:

$$I_{BH} = k \cdot I_{D30sat} + I_{BL} \quad (12)$$

where k is the ratio between the aspect ratio of M_{25} and M_{24} , and M_{27} and M_{26} , M_{28} . The higher threshold for I_{LOAD} is:

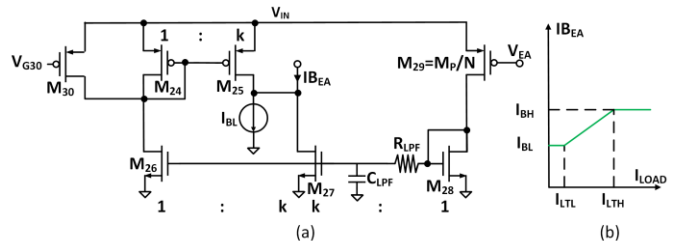


Fig. 5 (a) Error Amplifier Bias Shaper (EABS) simplified schematic and (b) I/O characteristic as function of the LDO load current.

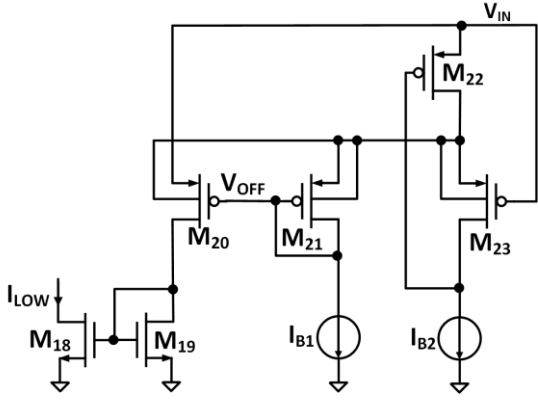


Fig. 6 Corner-tracking load current generator: simplified schematic.

$$I_{LTH} = N \cdot I_{D30sat} \quad (13)$$

With a moderate load, i.e. I_{LOAD} lower than I_{LTH} , the bias current depends almost linearly on the load current:

$$I_{BEA} = \frac{k}{N} \cdot I_{LOAD} + I_{BL} \quad (14)$$

Finally, with a very light load, I_{BEA} reaches a lower plateau at I_{BL} . This occurs for I_{LOAD} much lower than $(I_{BL} \cdot N / k)$. In that condition, all devices but the I_{BL} current generator are off, hence limiting the current consumption of the bias shaper to the leakage currents of the PMOS devices in Fig. 5(a).

In our design I_{BL} was set to 10 nA and I_{D30sat} to 16 nA with $k=8$ and $N=3960$, leading to I_{BL} and I_{BH} in Fig. 5(b) equal to 10 nA and 140 nA, respectively.

The low-pass filter $R_{LPF}-C_{LPF}$ (65 k Ω -370 fF) attenuates the kickback noise at the input reference pin and improves the transient behavior at the high-to-low load variation. Indeed in presence of a fast increase of the load current, the filter limits the slew-rate of the EA bias current and, consequently, of the voltage of shared sources of M_1 and M_2 , and of the drain of M_5 . It is worth to notice that the proposed solution, with the adaptive biasing circuits driven by the EA output, maintains better transient performance than conventional solutions, even in the presence of the above filter. Indeed, the R-C time constant is much smaller than the equivalent time constant at the buffer output at light-load conditions, due to the high value of R_{ob} from (4).

In presence of a high-to-low load transition, without the added filter the bias current would be suddenly reduced, because of the fast adaptive loop. The consequent degradation of the transient behavior is here avoided thanks to the filter, which allows maintaining a relatively high bias current during the settling of the LDO output.

C. Corner-tracking Load Current Generator

The absence of the resistive voltage divider as the feedback circuit, requires a block providing the pass device with the bias current. The absolute minimum bias for M_P corresponds to its own leakage current. Indeed, if the overall load current is lower than the leakage, the LDO feedback loop is not able to control the output voltage. Since the leakage current exhibits a huge variation over the process and temperature design space, setting the load current to the maximum leakage would strongly worsen the overall quiescent current of the regulator in typical conditions. This design problem has been solved by means of the corner-tracking bias block, shown in

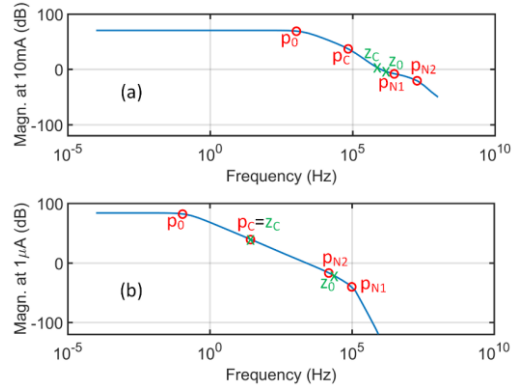


Fig. 7. Simulated loop-gain (module) of the LDO with unity feedback-factor: (a) high-load conditions and (b) light load with pole-zero cancellation.

Fig. 6 and connected to the LDO output, as in Fig. 3. This circuit implements a low-power replica of the DFVF buffer (M_{21} - M_{23}) without the adaptive bias feature and driving a scaled replica of the pass device, M_{20} . A constant bias (i.e. I_{B1} and I_{B2}) corresponding to the minimum bias current of the main ABDFVF is used here, with the input connected to the unregulated supply, V_{IN} . Therefore, the drain current of M_{20} is a scaled copy of the leakage current of the pass device, M_P . Finally, transistors M_{18} - M_{20} mirror to the output the generated corner-dependent load current I_{LOW} . It is worth to notice that this solution always provides the pass device with the minimum bias current, thus achieving the minimum overall quiescent current.

IV. FREQUENCY COMPENSATION STRATEGY

Maintaining a suitable stability margin in a linear regulator is a critical design task if the load current exhibits a broad range, starting from the open-load condition. If an off-chip capacitor is used for stabilization, the dominant pole of the loop gain is due to that capacitance, while the second pole, being related to the gate capacitance of the pass device, usually occurs before the UGF of the loop-gain. A phase margin in excess of 45° can be achieved by means of a compensation zero within the unity-gain bandwidth, which is introduced by the effective series resistance (ESR) of the off-chip load capacitor [19]. Nevertheless, the tolerance affecting the ESR makes this technique almost useless if an adequate stability margin must be maintained at light load [20].

A better solution is to link the compensation zero to the UGF, which in turns depends on the load current, temperature and process parameters. This is achieved by means of a shunt R-C network, placed at the output of the error amplifier (Z_Z

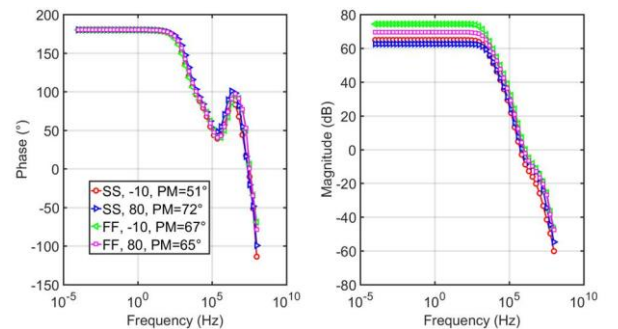


Fig. 8. Simulated loop gain at high-load condition over MOS corners and temperatures (-10°C and 80°C).

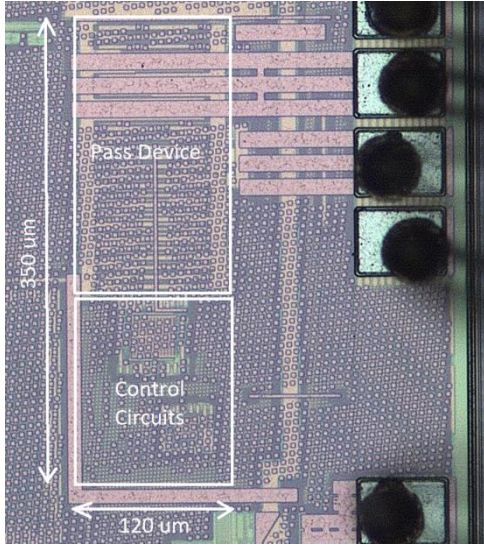


Fig. 9. Chip photograph.

in Fig. 2). The resistive part of Z_Z is linked to the drain-source resistance of M_P , which sets the value of the dominant pole [21]. As shown in Fig. 3 the compensation network is implemented with the on-chip capacitor, C_Z , and a transistor, M_Z , which is biased in the linear region and with the same gate-source voltage of M_P . Therefore, its drain-source resistance exhibits an inverse dependence on the load current, thus leading to a UGF-tracking zero. Even if this compensation technique is promising for improving the stability of ultra-low power LDOs, a buffer with a low output resistance is generally mandatory. As discussed in the previous section, the buffer can be a real bottleneck if the LDO must handle a sub-1 V unregulated supply. The required performance was achieved in the proposed design by a rail-to-rail DFVF buffer.

The approximate expressions of the most relevant poles and zeroes of the LDO loop gain are obtained by circuit analysis:

$$p_0 \approx -\frac{1}{r_{dsP} \cdot C_L} \quad (15)$$

$$p_C \approx -\frac{1}{C_Z \cdot (R_{OA} + R_Z)} \quad (16)$$

$$p_{N1} \approx -\frac{R_Z^{-1} + R_{OA}^{-1}}{C_{IB}} \quad (17)$$

$$p_{N2} \approx -\frac{1}{R_{OB} \cdot C_{gsP}} \quad (18)$$

$$z_C = -\frac{1}{C_Z \cdot R_Z} \quad (19)$$

$$z_0 = -\frac{1}{C_L \cdot (R_{ESR} + R_0)} \quad (20)$$

where r_{dsP} and C_{gsP} are the drain-source resistance and gate capacitance of M_P , C_{IB} and R_{OB} are the input capacitance and the output resistance of the buffer, ESR is the effective series resistance of capacitor C_L , R_Z is the drain-source resistance of M_Z , and R_{OA} is the output resistance of the Error Amplifier:

$$R_{OA} = \frac{1}{r_{ds10}^{-1} + r_{ds8}^{-1}} \quad (21)$$

It is worth to notice that the small-value on-chip resistor R_0 , partially desensitizes the frequency of z_0 to ESR. In the analysis above, the pole due to the body driving by the DFVF was not considered. Indeed such pole is expected to be located at a higher frequency than p_{N2} since the equivalent resistance at the source of M_{15} is lower than R_{ob} and the well-to-substrate junction capacitance of the pass device is lower than its gate capacitance.

In Fig. 7(a) the plot of the LDO loop gain is shown for the case of high load current. If the current is progressively reduced, both the tracking zero (z_C) and p_{N1} move to lower frequencies with the dominant pole, p_0 , because of the approximate inverse dependence of R_Z on I_{LOAD} . The behavior of p_C is quite different in the high-to-medium load current range since R_{OA} is much higher than R_Z and independent from I_{LOAD} , because of the current-limiting behavior of the EABS. Therefore, p_C is almost constant until, at light load, R_Z approaches R_{OA} . If the current is further decreased, both p_C and z_C exhibit almost the same dependence on R_Z and, hence, on I_{LOAD} , leading to a pole-zero cancellation, Fig. 7(b). Furthermore, because of the adaptive bias of the buffer, R_{OB} tracks I_{LOAD} and thus p_{N2} moves at lower frequencies with p_0 .

The simulated loop gain of the LDO at the maximum load current and at the extreme MOS corners and temperatures (i.e. -10°C and 80°C) is shown in Fig. 8. The reduction of the stability margin at the slow and minimum temperature corner is mainly ascribed to M_{13} in the ABDFVF buffer that is pushed to the limit of the saturation region, thus affecting the value of R_{ob} as discussed in Section III.A.

A further benefit of the implemented compensation is a relevant improvement of the PSR. Indeed, any medium-to-high frequency ripple affecting the input supply is coupled to the gate through M_Z - C_Z and the buffer. Therefore, as long as the gain of the buffer is close to one, the source-gate voltage of the pass device is not affected by that ripple, leading to a high PSR.

V. EXPERIMENTAL RESULTS

The chip has been fabricated in the TSMC 55nm CMOS process and the active area of the circuit is 0.042mm^2 . A photograph of the die is shown in Fig. 9. The relatively large area is due to the design optimization for minimum I_Q and to the 0.8 V supply. Indeed, only thick-oxide (I/O) devices were

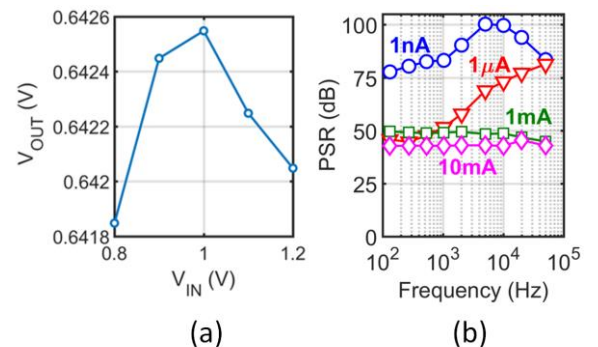


Fig. 10. (a) Measured line regulation at 100 μA load current and (b) PSR for $V_{REF}=600\text{ mV}$ and $V_{IN}=800\text{ mV}$.

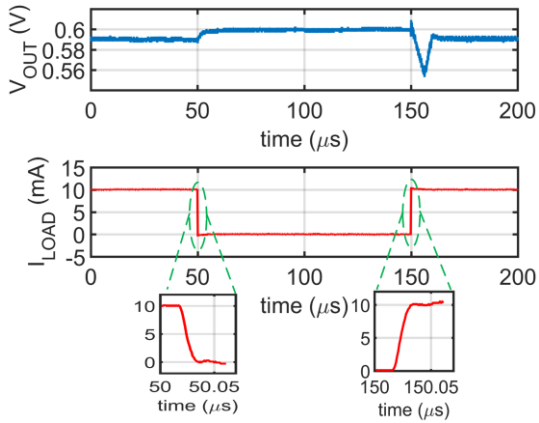


Fig. 11. Measured transient load regulation at $V_{REF}=600\text{mV}$ and $V_{IN}=800\text{mV}$.

used due to their lower leakage current than core devices.

All the measurements have been performed with a load capacitor of $1\ \mu\text{F}$. As shown in Fig. 10(a), a good DC line regulation is insured at $600\ \text{mV}$ voltage reference and $100\ \mu\text{A}$ load current. Furthermore, the measured DC line regulation is $0.5\ \text{mV/V}$ at $V_{REF}=600\ \text{mV}$ (supply varied from $0.8\ \text{V}$ to $1.2\ \text{V}$). As shown in Fig. 10(b), the LDO PSR remains very high over a wide range of frequency and load currents. Indeed, even varying the load current 10^7 times (from $1\ \text{nA}$ to $10\ \text{mA}$), the minimum PSR from DC to $50\ \text{kHz}$ is $42.7\ \text{dB}$ at $800\ \text{mV}$ supply and $V_{REF}=600\ \text{mV}$. At light load conditions the PSR increases of about $25\ \text{dB}$ with frequency. This is due to the drain-source resistance of M_P that becomes very high at those load conditions. According to the model in [22] this resistance, combined with the load capacitance leads to a high-pass behavior in the low-frequency range.

In Fig. 11 the transient response of the proposed LDO is shown for a reference voltage of $600\ \text{mV}$ and an input voltage of $800\ \text{mV}$. The current is changed from $10\ \text{mA}$ to $100\ \mu\text{A}$ and then to $10\ \text{mA}$ again. The current rise and fall times are about $20\ \text{ns}$, as shown in the zooms at the bottom of Fig. 11. A voltage drop of $70\ \text{mV}$ is measured, leading to a figure of merit $\text{FOM-t} = C_L I_Q \Delta V / \Delta I^2$ [23] of $11.4\ \text{ps}$.

The comparison with the state of art is shown in Table I.

TABLE I
COMPARISON WITH STATE OF ART

	[5]	[6]	[7]	[24]	[15]	[13]	This work	Unit
Technology	180	350	130	N.A.	N.A.	250	55	nm
Minimum input voltage	1.4	1.05	1.2	2.3	3.5	1.5	0.8	V
Output voltage	1.2	0.9	1	1.8	3	1 - 3	0.6	V
Maximum load current	50	50	5	50	150	150	10	mA
DC Load regulation	0.14	0.06	N.A.	2.25	0.2	0.17	1.05	mV/mA
DC Line regulation	7.25	N.A.	N.A.	4.5	15	N.A.	0.5	mV/V
Active area	0.03	0.05	0.002	N.A.	N.A.	0.108	0.042	mm ²
Trans. Drop (ΔV_{OUT})	18	7	200	350	545	160	70	mV
Trans. Load Variation (ΔI_{LOAD})	50	50	5	50	10	150	10	mA
Load current edge time	10	10	200	1000	N.A.	10	20	ns
FOM-t	3.04	10.6	N.A.	490	4800	8.8	11.4	ps
FOM-tV	6.0	11.7	N.A.	2590	58800	19.8	7.3	ps
Load capacitor	0.47	1	N.A.	1	2.2	1	1	μF
Min. PSR from DC to $50\ \text{kHz}$	44	50	70	8	8	13	42.7	dB
Quiescent current	0.9	4.04	99	3 *	0.4 **	1.24	0.016	μA

* For fair comparison quiescent current is reduced of $1\ \mu\text{A}$ with respect to the reference, because it contains also a bandgap reference.

** For fair comparison quiescent current is reduced of $100\ \text{nA}$ with respect to the reference, because it contains also an ultra-low-power bandgap reference.

The proposed LDO exhibits the lowest minimum supply voltage and quiescent current while being well aligned to other performance parameters shown in the literature. FOM-t is not the best if compared to other reported design, since [5], [6], [13] show better FOM-t. However, they all have larger voltage supplies and the regulator with the lowest supply voltage i.e. $1.05\ \text{V}$, among those three references, is the one with the highest FOM-t ($10.66\ \text{ps}$) [6]. This is not happening by case, but due to the fact that, for operating the LDO with the same maximum current at low supply voltages, its pass device needs to be larger, leading to larger parasitic capacitance to drive and, hence, a worst FOM-t. This is an intrinsic weakness of this widely used parameter for comparing low-voltage LDO designs. For this reason, FOM-t is modified as FOM-tV for taking into account the gate capacitance penalty occurring with the scaling down of the supply voltage:

$$\text{FOM-tV} = (C_L \cdot I_Q \Delta V / \Delta I^2) \cdot (V_{IN} / 1\ \text{V})^2 \quad (22)$$

Indeed, at high currents, the output device is biased in S.I. and, hence, the gate capacitance is inversely proportional to the square of the maximum overdrive of the pass device, i.e. $(V_{IN} + V_{TP})^2$, at a fixed value of maximum I_{LOAD} . Therefore, an accurate definition of the FOM-tV would require to multiply the FOM-t for $(V_{IN} + V_{TP})^2$, leading to an impractical figure-of-merit, since the value of V_{TP} is seldom reported. For this reason, the definition in (22) was preferred, even if the penalty caused by the lower supply is not completely de-embedded.

The scatter plots in Fig. 12 show a comparison with best-in-class low- I_Q LDOs in terms of FOM-tV, vs. I_Q and minimum PSR from DC to $50\ \text{kHz}$ (PSR_{MIN}) vs. I_Q [2], [5], [6], [9], [10], [13], [15], [24]–[26]. The achieved FOM-tV is the lowest reported in the literature after [5] and [10]. It is worth to notice that [5] exhibits more than $10\times$ quiescent current, whereas the outstanding performance of the cap-less LDO in [10] are achieved with a dynamic biasing approach, requiring calibration and causing a significant dependence of the quiescent current on the input voltage. Finally, the plot in

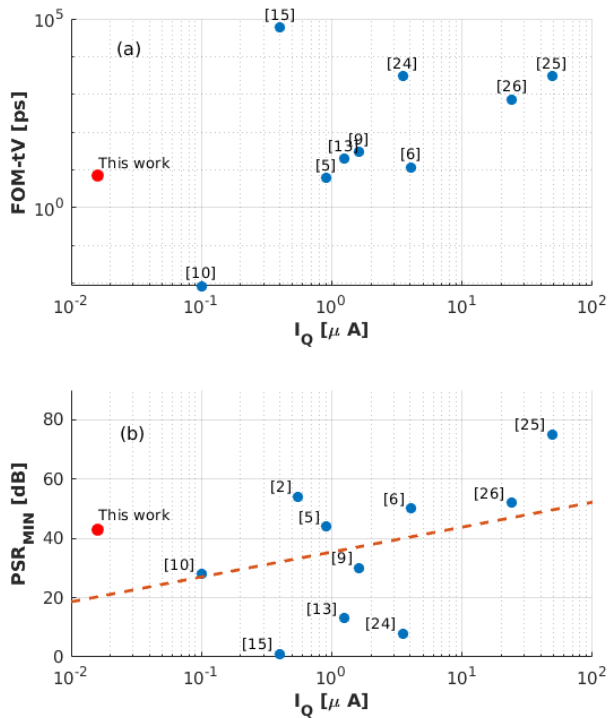


Fig. 12. Scatter plots comparing the proposed LDO with best-in-class low-power regulators. PSR_{MIN} is the minimum PSR over the 0-50 kHz range.

Fig. 12(b) shows that the achieved PSR is similar to that of other designs featuring two orders of magnitude higher I_Q .

VI. CONCLUSION

A low-drop-out regulator operating down to 0.8 V input with a quiescent current of 16 nA has been presented. This extremely low I_Q was achieved by extending the concept of adaptive bias to all the LDO blocks and by means of a corner-tracking bias generator for the output device. The transient behavior, line regulation, and PSR are not impaired by the low- I_Q thanks to a bias shaper, which limits by design the maximum step of the bias current and exhibits an almost linear dependence on the load current with moderate loads. Furthermore, the innovative driving concept for the adaptive bias generator provides relevant advantages for the transient behavior with a low-to-high step of the load current. A key block of the proposed design is the buffer, which is based on an adaptively biased DFVF, featuring zero DC voltage shift, rail-to-rail behavior over the huge load range and an additional output for driving the bulk terminal of the output transistor. Therefore, concurrent FBB and bulk modulation were implemented without any additional amplifier. An adequate stability margin was achieved over the load, supply, temperature range, and process corner by means of a UGF-tracking compensation circuit, which, as additional benefits, boosts the PSR of the LDO with respects to other compensation techniques.

VII. REFERENCES

- [1] R. J. M. Vullers, R. v. Schaijk, H. J. Visser, J. Penders, and C. V. Hoof, "Energy Harvesting for Autonomous Wireless Sensor Networks," *IEEE Solid-State Circuits Mag.*, vol. 2, no. 2, pp. 29–38, 2010.
- [2] M. Konijnenburg *et al.*, "A Multi(bio)sensor Acquisition System With Integrated Processor, Power Management, 8x8 LED Drivers, and Simultaneously Synchronized ECG, BIO-Z, GSR, and Two PPG Readouts," *IEEE J. Solid-State Circuits*, vol. 51, no. 11, pp. 2584–2595, 2016.
- [3] R. Mohan, S. Zaliasl, G. Gielen, C. Van Hoof, N. Van Helleputte, and R. F. Yazicioglu, "A 0.6V 0.015mm² time-based biomedical readout for ambulatory applications in 40nm CMOS," in *2016 IEEE International Solid-State Circuits Conference (ISSCC)*, 2016, pp. 482–483.
- [4] G. A. Rincon-Mora and P. E. Allen, "A low-voltage, low quiescent current, low drop-out regulator," *IEEE J. Solid-State Circuits*, vol. 33, no. 1, pp. 36–44, 1998.
- [5] A. Maity and A. Patra, "Design and Analysis of an Adaptively Biased Low-Dropout Regulator Using Enhanced Current Mirror Buffer," *IEEE Trans. Power Electron.*, vol. 31, no. 3, pp. 2324–2336, 2016.
- [6] Y. Lam and W. Ki, "A 0.9V 0.35 μ m Adaptively Biased CMOS LDO Regulator with Fast Transient Response," in *2008 IEEE International Solid-State Circuits Conference - Digest of Technical Papers*, 2008, pp. 442–626.
- [7] K. Keikhosravy and S. Mirabbasi, "A 0.13- μ m CMOS Low-Power Capacitor-Less LDO Regulator Using Bulk-Modulation Technique," *IEEE Trans. Circuits Syst. I Regul. Pap.*, vol. 61, no. 11, pp. 3105–3114, 2014.
- [8] Y.-S. K. Park, Kyeong-Hyeon, Yang, Il-Suk, Koo, "A Design of Low-dropout Regulator with Adaptive Threshold Voltage Technique," *Journal Semicond. Technol. Sci.*, vol. 18, no. 2, pp. 287–294, 2018.
- [9] A. Maity and A. Patra, "A Hybrid-Mode Operational Transconductance Amplifier for an Adaptively Biased Low Dropout Regulator," *IEEE Trans. Power Electron.*, vol. 32, no. 2, pp. 1245–1254, 2017.
- [10] Y. Huang, Y. Lu, F. Maloberti, and R. P. Martins, "Nano-Ampere Low-Dropout Regulator Designs for IoT Devices," *IEEE Trans. Circuits Syst. I Regul. Pap.*, vol. 65, no. 11, pp. 4017–4026, 2018.
- [11] Y. Lu, C. Li, Y. Zhu, M. Huang, U. S., and R. P. Martins, "A 312 ps response-time LDO with enhanced super source follower in 28 nm CMOS," *Electron. Lett.*, vol. 52, no. 16, pp. 1368–1370, 2016.
- [12] R. G. Carvajal *et al.*, "The flipped voltage follower: a useful cell for low-voltage low-power circuit design," *IEEE Trans. Circuits Syst. I Regul. Pap.*, vol. 52, no. 7, pp. 1276–1291, 2005.
- [13] R. Magod, B. Bakkaloglu, and S. Manandhar, "A 1.24 μ A Quiescent Current NMOS Low Dropout Regulator With Integrated Low-Power Oscillator-Driven Charge-Pump and Switched-Capacitor Pole Tracking Compensation," *IEEE J. Solid-State Circuits*, vol. 53, no. 8, pp. 2356–2367, 2018.
- [14] X. Ma, Y. Lu, and Q. Li, "A Fully-Integrated LDO with 50-mV Dropout for Power Efficiency Optimization," *IEEE Trans. Circuits Syst. II Express Briefs*, p. 1, 2019.
- [15] "TPS783 500-nA IQ, 150-mA, Ultralow Quiescent Current Low-Dropout Linear Regulator," *Texas Instruments*, 2017. [Online]. Available: <http://www.ti.com/lit/ds/symlink/tps783.pdf>. [Accessed: 23-Apr-2019].
- [16] D. J. Allstot, "A precision variable-supply CMOS comparator," *IEEE J. Solid-State Circuits*, vol. 17, no. 6, pp. 1080–1087, 1982.
- [17] R. Wang and R. Harjani, "Partial positive feedback for gain enhancement of low-power CMOS opas," *Analog Integr. Circuits Signal Process.*, vol. 8, no. 1, pp. 21–35, 1995.
- [18] T. Grotjohn and B. Hoeflinger, "A parametric short-channel MOS transistor model for subthreshold and strong inversion current," *IEEE Trans. Electron Devices*, vol. 31, no. 2, pp. 234–246, 1984.
- [19] G. A. Rincon-Mora and P. E. Allen, "Optimized frequency-shaping circuit topologies for LDOs," *IEEE Trans. Circuits Syst. II Analog Digit. Signal Process.*, vol. 45, no. 6, pp. 703–708, 1998.
- [20] M. Al-Shyokh, H. Lee, and R. Perez, "A Transient-Enhanced Low-Quiescent Current Low-Dropout Regulator With Buffer Impedance Attenuation," *IEEE J. Solid-State Circuits*, vol. 42, no. 8, pp. 1732–1742, 2007.
- [21] Y. Lu, R. H. Yao, D. Q. Huang, J. Su, J. Jiang, and W. Ki, "A low-dropout regulator with power supply rejection improvement by bandwidth-zero tracking," in *2014 IEEE Asia Pacific Conference on Circuits and Systems (APCCAS)*, 2014, pp. 105–108.
- [22] V. Gupta, G. A. Rincon-Mora, and P. Raha, "Analysis and design of monolithic, high PSR, linear regulators for SoC applications," in *IEEE International SOC Conference, 2004. Proceedings.*, 2004, pp. 311–315.
- [23] P. Hazucha, T. Karnik, B. A. Bloechel, C. Parsons, D. Finan, and S. Borkar, "Area-efficient linear regulator with ultra-fast load regulation," *IEEE J. Solid-State Circuits*, vol. 40, no. 4, pp. 933–

- 940, 2005.
- [24] "STLQ50 50 mA, 3 μ A supply current low drop linear regulator," *STMicroelectronics*, 2014. [Online]. Available: <https://www.st.com/en/power-management/stlq50.html>. [Accessed: 23-Apr-2019].
- [25] M. El-Nozahi, A. Amer, J. Torres, K. Entesari, and E. Sanchez-Sinencio, "High PSR Low Drop-Out Regulator With Feed-Forward Ripple Cancellation Technique," *IEEE J. Solid-State Circuits*, vol. 45, no. 3, pp. 565–577, 2010.
- [26] "LP5900 150-mA Ultra-Low-Noise LDO for RF and Analog Circuits," *Texas Instruments*, 2019. [Online]. Available: <http://www.ti.com/lit/ds/symmlink/lp5900.pdf>. [Accessed: 10-May-2019].



Nicola Adorni was born in Parma, Italy, in 1991. He received the M.S. degree in Electronic Engineering from the University of Parma, Parma, Italy, in 2017, with a master thesis on a low-power linear regulator. From 2017 to 2019 he worked for AMS on the development of CMOS Image Sensors, Antwerpen, Belgium. In 2019 he moved to e-peas, Mont-Saint-Guibert, Belgium, where he is currently working on the design of analog and mixed-signal blocks for ultra-low power energy harvesting solutions. His current interests include ultra-low power circuits and systems for energy harvesting applications.



Stefano Stanzione received the M.S. and the Ph.D. degree from the University of Pisa, Pisa, Italy, in 2006 and 2010, respectively. His Ph.D. work focused on the analog building blocks of autonomous UHF RFID tags. He joined the Holst Centre/imec, Eindhoven, The Netherlands, in 2010, where he is currently an Analog Design Engineer. His current research interests include ultra-low-power circuits for energy harvesting and battery management. Dr. Stanzione has been a member of the Analog Technical Program Sub-Committee of ISSCC between 2014 and 2018.



Andrea Boni received the M.S. degree in Electronics and the Ph.D. degree in Information Technologies from the University of Parma, Parma, Italy, in 1993 and 1997, respectively. From 1999 to 2002 he was a Research Assistant at the Dep.t of Information Engineering of the University of Parma. Since 2002 he has been Associate Professor of Electronics at the University of Parma, where he currently is the responsible of the Analog I.C. design group. He is the author of more than 80 scientific papers and holds one patent on a low-noise opamp. His research interests include the design of A/D converters, integrated sensor nodes, RFID devices, ultra-low power analog circuits, and auto-motive applications. Prof. Boni was a co-founder of Silis S.r.l., a University spin-off company involved in the design of high-performance analog and mixed signal integrated circuits. He has been in the technical committee of the Custom Integrated Circuits Conference.